HHS Public Access

Author manuscript

Acta Biomater. Author manuscript; available in PMC 2017 October 01.

Published in final edited form as:

Acta Biomater. 2016 October 1; 43: 282–291. doi:10.1016/j.actbio.2016.07.014.

A Prodrug Micellar Carrier Assembled from Polymers with Pendant Farnesyl Thiosalicylic Acid Moieties for Improved Delivery of Paclitaxel

Jingjing Sun[a,b,c,§], **Yichao Chen**[a,b,c,§], **Ke Li**[d], **Yixian Huang**[a,b,c], **Xiaofeng Fu**[e], **Xiaolan Zhang**[a,b,c], **Wenchen Zhao**[b], **Yuan Wei**[a,b,c], **Liang Xu**[d], **Peijun Zhang**[e], **Raman Venkataramanan**[b], and **Song Li**[a,b,c,*]

[a]Center for Pharmacogenetics, University of Pittsburgh, Pittsburgh, PA, 15261, USA

[b]Department of Pharmaceutical Sciences, School of Pharmacy, University of Pittsburgh, Pittsburgh, PA, 15261, USA

[c]University of Pittsburgh Cancer Institute, University of Pittsburgh, Pittsburgh, PA, 15261, USA

[d]Departments of Molecular Biosciences and Radiation Oncology, and University of Kansas Cancer Center, University of Kansas, Lawrence, Kansas 66045, United States

[e]Department of Structural Biology, School of Medicine, University of Pittsburgh, Pittsburgh, PA 15261, USA

Abstract

In order to achieve enhanced and synergistic delivery of paclitaxel (PTX), a hydrophobic anticancer agent, two novel prodrug copolymers, $POEG_{15}$-*b*-$PFTS_6$ and $POEG_{15}$-*b*-$PFTS_{16}$ composed of hydrophilic poly(oligo(ethylene glycol) methacrylate) (POEG) and hydrophobic farnesylthiosalicylate (FTS, a nontoxic Ras antagonist) blocks, were synthesized. Both POEG-*b*-PFTS polymers were able to form micelles with intrinsic antitumor activity *in vitro* and *in vivo*. Employing these micelles as a carrier to load PTX, their drug loading capacity, stability, *in vivo* biodistribution and tumor inhibition effect were evaluated. PTX/$POEG_{15}$-*b*-$PFTS_{16}$ mixed micelles exhibited an excellent stability of 9 days at 4°C with a PTX loading capacity of 8.2%, which was more effective than PTX/$POEG_{15}$-*b*-$PFTS_6$ mixed micelles. *In vivo* biodistribution data showed that DiR-loaded POEG-*b*-PFTS micelles were more effectively localized in the tumor than in other organs. Moreover, both PTX/POEG-*b*-PFTS micelles showed significantly higher antitumor activity than Taxol in a 4T1.2 murine breast tumor model, and the tumor inhibition and animal survival followed the order of PTX/$POEG_{15}$-*b*-$PFTS_{16}$ > PTX/$POEG_{15}$-*b*-$PFTS_6$ > $POEG_{15}$-*b*-$PFTS_{16}$ > Taxol ≈ $POEG_{15}$-*b*-$PFTS_6$. Our data suggest that POEG-*b*-PFTS micelles are a promising anticancer drug carrier that warrants more studies in the future.

*Author for correspondence: Song Li, M.D., Ph.D., Phone: 412-383-7976, Fax: 412-648-1664, sol4@pitt.edu.

§The author made an equal contribution in this work. All authors have given approval to the final version of the manuscript.

Graphical Abstract

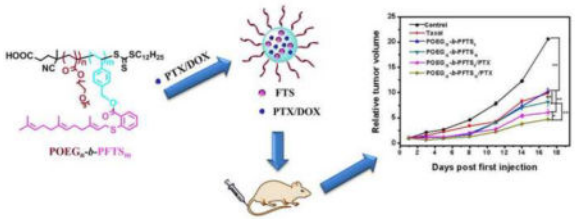

Keywords

farnesyl thiosalicylic acid (FTS); prodrug micelles; paclitaxel; doxorubicin; co-delivery

1. Introduction

Taxol is a clinical formulation of paclitaxel (PTX), which has been used to treat a range of malignant tumors. However, lack of tissue-specificity, hypersensitivity reactions and other side effects such as neuropathy limited its application [1–3]. To overcome these problems, various drug delivery systems such as liposomes, micelles, polymersomes and hydrogels have been developed [4–6]. Among them, polymeric micelles whose core-shell structures can encapsulate the hydrophobic drugs and prolong their circulation time in the blood have gained considerable attention. The small size of polymeric micelles will allow encapsulated drug to be effectively and passively delivered to tumor tissues via an enhanced permeability and retention (EPR) effect [7]. However, most polymeric micellar carriers are constructed by a large amount of pharmacologically inert materials which might increase the cost and lead to potential toxicity *in vivo*.

Micelles that are based on properly designed PEG-hydrophobic drug conjugates (prodrugs) possess natural amphiphilic properties and can serve as dual-functional carriers for co-delivery of other hydrophobic drugs [8–11]. Due to the antitumor activity of carrier materials, they can facilitate potential synergistic effects with the co-delivered drugs [12–14]. In addition, this system might provide a programmable loading and release of various drug components via both chemical conjugation and physical encapsulation.

It has been known that the development and growth of many tumors are related to the chronic activation of Ras signaling. S-trans,trans-farnesylthiosalicylic acid (FTS) is a nontoxic Ras antagonist, which could disassociate active Ras proteins from cell membrane selectively, leading to Ras dependent tumor regression [15–20]. Besides, FTS exhibits anti-inflammatory activity [21, 22]. Clinically, FTS (Salirasib) has been approved for phase I ~ II trials, and a phase I study reported that FTS was well tolerated and effective in relapsed hematological malignancies [23,24]. Inspired by the function of FTS, our group developed a series of prodrug micellar carriers which were based on PEG conjugates with two molecules of FTS [25–27]. It was shown that the PEG_{5K}-FTS_2 carrier well retained the biological activity of FTS upon examination in cultured tumor cells. Furthermore, PTX/PEG_{5K}-FTS_2 formulation showed a significantly higher anti-cancer activity than that of Taxol [25]. Nevertheless, the PTX loading capacity and micellar stability need to be improved.

Recent studies have shown that formulation stability, drug loading capacity and drug release rate of polymeric carriers can be regulated by modulating the size of hydrophobic cores [28–31]. Our previous work also demonstrated that a PEG conjugate with four FTS molecules (PEG_{5K}-FTS_4) could form more stable PTX-loaded micelles with higher PTX loading capacity than PEG conjugates with two FTS molecules (PEG_{5K}-FTS_2) [32]. Furthermore, *in vivo* study showed that PTX/PEG_{5K}-FTS_4 mixed micelles exhibited higher anti-tumor activity compared to PTX/PEG_{5K}-FTS_2 micelles. Nonetheless, due to the relatively low FTS contents in either PEG_{5K}-FTS_2- or PEG_{5K}-FTS_4-based carriers, the amounts of FTS that can be delivered to tumor tissues are limited, which limits the contribution of carriers-associated biological activity to the overall antitumor activity of drug-loaded micelles. This has promoted us to explore new prodrug micellar systems with further increased sizes of FTS-based hydrophobic core. Generally, most reports employed postmodification method by which a drug was chemically attached to a polymer backbone to construct prodrug micelles [33, 34]. However, this method often involves many synthesis steps which is a little complicated. In addition, because of steric hindrance, some reactive groups might remain in the polymers following conjugation, which might cause destruction of micelle structure or side effects *in vivo* through reacting with bioactive molecules [35]. Recently, polymerization of drug-based monomer has been developed as a facile strategy to obtain well-defined prodrug amphiphilic polymers [36, 37]. But most reports largely focus on the synthesis methods and the biophysical properties (e.g. micelle formation, enzymatic degradability, drug release, etc.) of prodrugs themselves [38, 39]. There is limited information about their anti-tumor activity and delivery function as prodrug carriers *in vitro* and *in vivo*. Therefore, there is still a need to develop more anti-tumor prodrug amphiphiles through development and subsequent polymerization of new drug-based monomers, and investigate their potential as a dual-functional drug delivery system.

In this work, we designed a novel FTS-based vinyl monomer that was easy to be synthesized and could be readily polymerized by reversible addition-fragmentation transfer (RAFT) polymerization to give well-defined diblock copolymers with a hydrophilic POEG block and a hydrophobic FTS block. The new polymers could be self-assembled into prodrug micelles and their sizes and structures were characterized. Employing these polymers as a PTX delivery carrier, the drug loading and release were further evaluated. Finally, the antitumor activity of carriers alone and PTX-loaded micelles was investigated *in vitro* and *in vivo*.

2. Materials and methods

2.1. Materials

FTS was synthesized and purified following a published literature [18]. Vinylbenzyl chloride, 4-Cyano-4-[(dodecylsulfanylthiocarbonyl)sulfanyl]pentanoic acid, oligo(ethylene glycol) methacrylate OEGMA (average Mn=500), 2, 2-Azobis(isobutyronitrile) (AIBN), trypsin-EDTA solution, 3-(4,5-dimethylthiazol-2-yl)-2,5-diphenyl tetrazolium bromide (MTT) and Dulbecco's Modified Eagle's Medium (DMEM) were all bought from Sigma-Aldrich (MO, U. S. A.). AIBN was purified by recrystallization in anhydrous ethanol. Paclitaxel was purchased from AK Scientific Inc. (CA, U. S. A.). DOX·HCl was purchased from LC Laboratories (MA, USA). Fetal bovine serum (FBS) and penicillin-streptomycin

solution were purchased from Invitrogen (NY, U. S. A.). Cell culture and animals were similarly handled as described before [32].

2.2. Synthesis of FTS-monomer

FTS (377.3 mg, 1.1 mM), vinylbenzyl chloride (167.2 mg, 1.1 mM) and K_2CO_3 (0.55 g, 5.5 mM) were dissolved in 5.5 mL DMF and immersed into an oil bath at 50°C. After 4 h, 5 mL water was added to the cooled mixture, and then 100 mL CH_2Cl_2 was added to extract the product. The organic phase was collected and washed by water and brine. After evaporation, silica gel column chromatography was used to purify the crude product with petroleum ether/diethyl ether (v/v, 8/1) as the elution. Colorless oil FTS-monomer was obtained with a 53% yield.

2.3. Synthesis of POEG macroCTA

OEGMA (3.05 g, 6.1 mmol), 4-Cyano-4-[(dodecylsulfanylthiocarbonyl)sulfanyl]pentanoic acid (120 mg, 0.305 mmol), AIBN (10 mg, 0.062 mmol) and 5 mL dried 1,4-dioxane were added in a Schlenk tube, and deoxygenated by free-pump-thawing for three times. Then under N_2 protection, the mixture was put into an oil bath thermostated at 85°C. After 3 h, the tube was put into liquid nitrogen to quench the reaction and the mixture was then precipitated in diethyl ether for 3 times. After vacuum drying, the yellow oil product POEG was obtained. The conversion was 75% as determined by ^{1}H NMR spectroscopy.

2.4. Synthesis of POEG-b-PFTS polymers

POEG macroCTA (140 mg, 0.0186 mmol), FTS-monomer (186 mg, 0.400 mmol), AIBN (1 mg, 0.0062 mmol) and 2 mL dried 1, 4-Dioxane were added in a Schlenk tube, and deoxygenated by free-pump-thawing for three times. The mixture was then protected under N_2 and immersed into an oil bath at 90°C. After 24 h, the tube was put into liquid nitrogen to quench the reaction and the mixture was precipitated in hexane for 3 times, and dried in vacuum.

2.5. Characterization of the synthesized monomer and polymers

^{1}H NMR spectrum was conducted on a Varian 400 FT-NMR spectrometer at 400.0 MHz with $CDCl_3$ as the solvent. Molecular weight (M_n and M_w) and polydispersity index (M_w/M_n) of the synthesized polymers were measured by gel permeation chromatography (GPC) equipped with a Waters 2414 refractive index detector, a Waters 515 HPLC pump and a Waters 717 Plus Autosampler. THF was used as the eluent with a flowing rate of 1.0 mL/min at 35°C. A series of commercial polystyrene standards with narrow molecular weight distribution were applied to calibrate the GPC elution traces.

2.6. Preparation and characterization of PTX- and DOX-loaded micelles

PTX (5 mg/mL in dichloromethane) and POEG-*b*-PFTS polymers (50 mg/mL in dichloromethane) were mixed under different carrier/drug ratios. After removing the dichloromethane, a thin film was formed. PTX-loaded micelles were formed by adding DPBS solution to hydrate the thin film followed by gentle votexing. To load DOX into the POEG-*b*-PFTS micelles, DOX·HCl was first dissolved in a mixture of chloroform ($CHCl_3$)/

methanol (MeOH) (1:1, v/v) containing triethylamine (3 equiv) to remove HCl. DOX-loaded POEG-*b*-PFTS micelles were then similarly prepared. PTX loading efficiency was measured by high performance liquid chromatography (HPLC) and the DOX loading efficiency was examined by Waters Alliance 2695 Separations Module combined with Waters 2475 Fluorescence Detector (excitation, 490 nm; emission, 590 nm; gain, 3; sensitivity (FUFS), 10 000) as described before [25, 26]. Drug loading capacity (DLC) and drug loading efficiency (DLE) were calculated from the following equations:

$$\mathrm{DLC}\,(\%)\,[\text{weight of drug loaded}/(\text{weight of polymer}+\text{drug used})] \times 100$$
$$\mathrm{DLE}\,(\%) = (\text{weight of loaded drug}/\text{weight of input drug}) \times 100$$

The average diameter, size distribution and morphology of POEG-*b*-PFTS blank micelles and drug-loaded micelles were assessed by dynamic light scattering (DLS) and transmission electron microscopy (TEM).

2.7. Critical micelle concentration (CMC) and serum stability of POEG-b-PFTS micelles

The CMC values of POEG-*b*-PFTS micelles were measured with nile red as a fluorescence probe [40, 41]. In brief, 30 μL of a 0.05 mg/mL nile red solution in dichloromethane was added to each tube and then it was placed at room temperature overnight to remove solvent completely. Then 2 mL of POEG-*b*-PFTS micellar solution with different concentrations was added to each vial respectively. After 6 h, the emission spectra (570~720 nm) of the solutions were measured at an excitation wavelength of 550 nm and the peak intensities at 650 nm of the emission spectra were plotted versus polymer concentrations.

The serum stability of the polymers was evaluated by examining the FTS release in serum. The polymers were incubated with 50% serum (from rat) at 37 °C for 48 h. Then, methanol was added to extract the cleaved FTS for 3 times. After centrifugation at 12,000 rpm for 10 min, the supernatants were tested by MS analysis on a UPLC-QTOF MS system. FTS analysis was conducted on an Acquity UPLC BEH C18 column in negative mode with electrospray ionization.

2.8. In vitro PTX release

The kinetics of PTX release from PTX/POEG-*b*-PFTS mixed micelles was examined according to a previous report [42]. Briefly, 1 mL of PTX-loaded POEG-*b*-PFTS micelles or Taxol (1 mg PTX/mL) solution was transferred into a dialysis bag (MWCO = 3.5 kDa), and incubated in a tank with 50 mL PBS (PH = 7.4 or 5.5) containing 0.5% (w/v) Tween 80 as release medium, with gentle shaking at 37 °C. At specific time intervals, the PTX concentration in the dialysis bag was tested by HPLC at 227 nm wavelength.

2.9. In vitro cytotoxicity assay

In vitro cytotoxicity studies of POEG-*b*-PFTS polymers were carried out on both 4T1.2 mouse breast cancer cells and DU145 human prostate cancer cells. In brief, tumor cells were seeded into a 96-well plate at a density of 2000 cells/well and cultured overnight. Cells were challenged with various concentrations of blank POEG-*b*-PFTS micelles or free FTS at equivalent FTS concentrations for 72 h. MTT assay was performed as described before [25]

and cell viability was calculated with untreated cells as a control. A similar study was performed with PTX- or DOX-loaded POEG-*b*-PFTS micelles and compared with Taxol or free DOX at same concentrations of chemotherapy drugs.

2.10. Near-infrared fluorescence optical imaging

Two hundreds μL of DiR-loaded POEG-*b*-PFTS micelles with a DiR concentration of 0.4 mg/mL were injected into SCID mice bearing bilateral s.c. PC-3 xenografts. At indicated times, the mice were imaged by Multispectral FX PRO system (Carestream Molecular Imaging) at a 60 s exposure time with excitation at 730 nm and emission at 835 nm. The mice were anesthetized by isoflurane inhalation before imaging. After 96 h, the mice were euthanized by CO_2 overdose. The tumor and various organs were excised for ex vivo imaging.

2.11. In vivo therapeutic study

The *in vivo* antitumor efficacy of the POEG-*b*-PFTS-based drug delivery system was tested with a syngeneic 4T1.2 mouse breast cancer model [43]. 2×10^5 4T1.2 cells in 100 μL PBS were inoculated subcutaneously at the lower right flank of female BALB/c mice. When the tumor volume reached around 50 mm^3, mice were divided into six groups (n=8) and PBS, POEG-*b*-PFTS blank micelles ($POEG_{15}$-*b*-$PFTS_6$ or $POEG_{15}$-*b*-$PFTS_{16}$), Taxol and PTX/POEG-*b*-PFTS micelles were i.v. injected into each group, respectively, at a PTX dose of 10 mg/kg. The treatments were performed every two days for a total of 5 times. Tumor sizes were measured every three days following the initiation of the treatment and mouse body weights were monitored as an indication of toxicity. The tumor sizes (V) were calculated by the equation: V= (length of tumor)× (width of tumor)^2/2.

In addition to following changes in tumor sizes, the survival was also examined. The end point of survival will be defined as animal death or when the implanted tumor reached a volume of ~1000 mm^3. The survival rate was plotted as KaplaneMeier curves and the median survival of mice was calculated.

2.12. Statistical analysis

Data are presented as mean ± standard deviation (SD). Two-tailed Student's T test or one-way analysis of variance (ANOVA) was used to compare two groups or multiple groups, respectively, and Newman-Keuls test was performed if the overall p-value is <0.05. Survival data were generated by the KaplaneMeier method and statistical significance was evaluated by ManneWhitney U-tests. In all statistical analyses, $p < 0.05$ is considered statistically significant.

3. Results and Discussion

3.1. Synthesis and characterization of the POEG-b-PFTS polymers

We have previously developed a series of PEG_{5K}-FTS_2 polymers as prodrug carriers for PTX delivery [25–27]. However, due to the low percentage of hydrophobic FTS moieties in the polymers, these carriers showed limited PTX loading capacity and formulation stability. In addition, although PTX-loaded micelles exhibited high anti-tumor activity, PEG-FTS_2

prodrug carriers alone showed minimal antitumor activity due to the low FTS loading capacity and thus limited amounts of FTS that can be delivered to the tumor tissues. This may limit the eventual synergistic action between PEG-FTS-based carriers and the co-delivered PTX. In order to overcome these problems, in this work, we designed and synthesized POEG-*b*-PFTS polymers with higher numbers of FTS moieties and investigated the impact of different amounts of FTS moieties on the delivery functions of carriers.

First, we designed and synthesized a new kind of FTS-based monomer where FTS was conjugated with vinylbenzyl chloride to form a hydrolyzable ester linkage as shown in Scheme 1. Then, the macro-chain transfer agent POEG was synthesized by RAFT polymerization of hydrophilic OEGMA monomer, which was further used to initiate the polymerization of hydrophobic FTS monomer, yielding the amphiphilic POEG-*b*-PFTS block copolymers. By varying the feeding ratio of FTS-monomer/macro-RAFT agent, POEG-*b*-PFTS copolymers with different PFTS block lengths ($POEG_{15}$-*b*-$PFTS_6$, $POEG_{15}$-*b*-$PFTS_{16}$, and $POEG_{15}$-*b*-$PFTS_{29}$) were prepared. Preliminary study showed that $POEG_{15}$-*b*-$PFTS_{29}$ formed precipitates in the course of micelle preparation (data not shown). This is likely due to the overly hydrophobic nature of $POEG_{15}$-*b*-$PFTS_{29}$. Therefore, subsequent studies were focused on $POEG_{15}$-*b*-$PFTS_6$ and $POEG_{15}$-*b*-$PFTS_{16}$ polymers. The structures of these polymers were confirmed by ^{1}H NMR (Fig. 1), and the average degree of polymerization (DP) of the FTS monomers were calculated by comparing the intensities of I_b and I_a. The characteristics of these POEG and POEG-*b*-PFTS polymers as determined by ^{1}H NMR and GPC were summarized in Table 1, which indicated the successful synthesis of the POEG-*b*-PFTS block copolymers with defined and controllable structures.

3.2. Physicochemical characterization of blank and PTX-loaded POEG-b-PFTS micelles

A simple film hydration method was used for preparing blank POEG-*b*-PFTS and PTX-loaded POEG-*b*-PFTS micelles. Fig. 2 & Table 2 showed the CMCs of $POEG_{15}$-*b*-$PFTS_6$ and $POEG_{15}$-*b*-$PFTS_{16}$ micelles. It was interesting to note that incorporation of sixteen FTS units led to a 3-fold decrease in CMC compared to $POEG_{15}$-*b*-$PFTS_6$. The low CMC of $POEG_{15}$-*b*-$PFTS_{16}$ (~2.7 mg/L) shall provide a good stability for the micelles upon dilution in blood stream after administration. DLS showed that $POEG_{15}$-*b*-$PFTS_6$ and $POEG_{15}$-*b*-$PFTS_{16}$ formed micelles with a diameter of 30 nm and 130 nm in aqueous solution, respectively (Table 2). TEM (Fig. 3A and 3C) and cryo-EM (Fig. S1) images further confirmed the spherical shape of POEG-*b*-PFTS micelles. Besides, the FTS loading is calculated to be 20.1% for $POEG_{15}$-*b*-$PFTS_6$ and 36.7% for $POEG_{15}$-*b*-$PFTS_{16}$ prodrug micelles (Table 2), which is significantly higher than that of previously reported PEG-FTS conjugates (11.3~20.4%) [25, 26, 32].

Since FTS is linked to the polymer by an ester bond, the serum stability of the polymers was evaluated by examining the FTS cleavage percentage in 50% serum. As shown in Fig. S2, only 0.4% and 0.2% FTS were cleaved from the $POEG_{15}$-*b*-$PFTS_6$ and $POEG_{15}$-*b*-$PFTS_{16}$ polymers in the serum, respectively, which indicated the good stability of POEG-*b*-PFTS polymers in serum. This is likely due to the fact that FTS is tightly packed in the hydrophobic core, limiting the digestion by the serum esterases.

We then examined and compared the PTX loading capacity and colloidal stability of the PTX-loaded POEG-*b*-PFTS micelles. As shown in Table 3 & Fig. 3B&D, PTX could be loaded into both POEG-*b*-PFTS micelles at a carrier/drug ratio as low as 10/1 (mg/mg). At this ratio, the $POEG_{15}$-*b*-$PFTS_{16}$ can achieve a PTX loading capacity of 8.2% and the PTX-loaded micelles were stable with no obvious changes in sizes or precipitation for 9 days at 4°C. In addition, upon increasing the carrier amount, the drug encapsulation efficiency and colloidal stability were further improved. It is also apparent that PTX-loaded $POEG_{15}$-*b*-$PFTS_{16}$ micelles showed better colloidal stability than $POEG_{15}$-*b*-$PFTS_6$ formulation at all carrier/drug ratios examined (Table 3). This improvement may be due to enhanced carrier/drug interactions provided by increased number of FTS hydrophobic motifs. In addition to PTX, several other commonly used chemotherapeutic agents including docetaxel, doxorubicin (DOX), gefitinib, and imatinib could be effectively loaded into POEG-*b*-PFTS prodrug carriers (Table 1 and data not shown). Table S1 and Fig. S3 showed the physicochemical characterization and TEM imaging of DOX-loaded POEG-*b*-PFTS micelles. Thus, the POEG-*b*-PFTS prodrugs may represent a versatile carrier for delivery of different kinds of anticancer drugs.

3.3. In vitro drug release

The release profile of PTX-formulated POEG-*b*-PFTS micelles was investigated with a dialysis method in DPBS (pH 7.4) with Taxol formulation as a control. As shown in Fig. 4, 45% of PTX was rapidly released from Taxol formulation in the first hour and around 60% of the total drug was released within 12 h. In comparison, less than 20% of PTX incorporated in the POEG-*b*-PFTS micelles was released in the first hour and a slow kinetics of release persisted for an extended period of 60 hours. The performance of PTX cumulative release follows the order of PTX/$POEG_{15}$-*b*-$PFTS_{16}$ > PTX/$POEG_{15}$-*b*-$PFTS_6$ > Taxol. Similar results were obtained when this experiment was conducted with an acidic (pH=5.5) release medium (Fig. S4). This sustained drug release is likely due to the strong carrier-drug interaction between PTX and POEG-*b*-PFTS carriers. $POEG_{15}$-*b*-$PFTS_{16}$ with more FTS units provided enhanced hydrophobic interaction, resulting in the most favorable release kinetics of PTX.

3.4. In vitro cytotoxicity of prodrug micelles and PTX/DOX-loaded micelles

The cytotoxicity of $POEG_{15}$-*b*-$PFTS_6$ and $POEG_{15}$-*b*-$PFTS_{16}$ was examined in 4T1.2 mouse breast cancer cells and DU-145 human prostate cancer cells with free FTS as a control. Cell viability was determined by MTT assay after 3 days of treatment with untreated cells as a control. As shown in Fig. 5, free FTS exhibited a concentration-dependent tumor inhibition effect. The two POEG-*b*-PFTS prodrug micelles were less active than free FTS at equivalent amount of FTS in both 4T1.2 and DU145 tumor cells (Fig. 5A, B). The cytotoxicity of POEG-*b*-PFTS was unlikely due to the surfactant effect since polymer micelles exhibited little hemolytic activity at even much higher concentrations (data not shown). The cytotoxicity shall likely come from the FTS cleaved from the polymer following intracellular uptake. The less effectiveness of POEG-*b*-PFTS in cytotoxicity was likely due to the limited FTS release in a relative short period of treatment. We can expect an enhanced cell killing effect with an extended treatment since the POEG-*b*-PFTS carriers alone showed significant tumor inhibition effect in a later *in vivo* study (Fig. 8).

Figure 6A&B show the cytotoxicity of Taxol and PTX-loaded POEG-*b*-PFTS micelles in 4T1.2 and DU145 cell lines. PTX formulated in POEG-*b*-PFTS micelles showed a cell killing effect that was comparable to that of Taxol control. The cytotoxicity of DOX-loaded micelles were also evaluated with free DOX·HCl as the control. As presented in Fig. 6C&D, DOX-loaded POEG-*b*-PFTS micelles exhibited similar cell killing effect compared to free DOX·HCl.

3.5. Near-infrared fluorescence optical imaging

In vivo biodistribution of POEG-*b*-PFTS micelles was investigated by near-infrared fluorescent optical imaging in a PC-3 human prostate cancer xenograft model. A highly penetrating hydrophobic fluorescence dye DiR was loaded into the POEG-*b*-PFTS micelles for tissue imaging. As shown in Fig. 7A, DiR-loaded POEG-*b*-PFTS micelles were largely concentrated at tumor sites. The signals could be detected at as early as 1 hour after injection and peaked at about 24 h. However, substantial amounts of micelles were still retained at tumor sites even 96 h later. No obvious tumor accumulation was detected in the mice treated with free DiR dye [44].

Tumors and major organs were harvested for ex vivo imaging and fluorescence quantification at 96 h post-injection. Significantly larger amounts of signals were observed in the tumor tissues compared to other major organs including lung, heart, liver, kidney and spleen (Fig. 7B). The enhanced micelle accumulation at tumor site other than other major organs/tissues was likely attributed to a strong enhanced permeability and retention (EPR) effect due to the small size (less or around 100 nm) of POEG-*b*-PFTS micelles and their excellent stability in blood stream. Fig. 7C showed that higher DiR signals were observed in tumors with DiR/$POEG_{15}$-*b*-$PFTS_{16}$ treatment compared to $POEG_{15}$-*b*-$PFTS_6$ formulation, suggesting $POEG_{15}$-*b*-$PFTS_{16}$ might serve as a better drug delivery system because of its enhanced stability and more effective tumor targeting in vivo.

3.6. In vivo therapeutic efficacy

The anti-tumor activity of PTX/POEG-*b*-PFTS mixed micelles was investigated by using an aggressive 4T1.2 mouse tumor model. It was demonstrated in Fig. 8A that Taxol formulation at a dose of 10 mg PTX/kg had a moderate tumor inhibition effect. Interestingly, $POEG_{15}$-*b*-$PFTS_6$ and $POEG_{15}$-*b*-$PFTS_{16}$ prodrug micelles alone showed comparable or further enhanced tumor inhibition effect compared to Taxol at day 17. It is likely that the antitumor activity of POEG-*b*-PFTS comes from the released FTS following the enzyme-mediated cleavage of the ester bond. This is quite different from our previous studies with PEG-FTS conjugates, in which the carriers alone showed minimal antitumor activity [25]. This is attributed to the fact that our new carriers allow delivery of sufficient amounts of FTS to the tumors due to the increased FTS moieties in POEG-*b*-PFTS polymers. It is also apparent that incorporation of PTX into POEG-*b*-PFTS micelles led to further improved anti-tumor activity. The superior anti-tumor activity of PTX/POEG-*b*-PFTS is likely attributed to the small size of the micelles, which allows them to efficiently penetrate and accumulate in the poorly vascularized tumors. Moreover, the potential combination effect of cleaved FTS and co-delivered PTX may also play a role in tumor inhibition. Overall, $POEG_{15}$-*b*-$PFTS_{16}$ micelles were more active than $POEG_{15}$-*b*-$PFTS_6$ micelles either by themselves or as mixed

micelles with PTX ($P<0.05$). More FTS units in $POEG_{15}$-*b*-$PFTS_{16}$ provided stronger carrier-drug interaction to achieve an improved stability (Table 3) and better targeting (Fig. 7) in vivo. In addition, more FTS will be delivered to tumors with $POEG_{15}$-*b*-$PFTS_{16}$ system than with $POEG_{15}$-*b*-$PFTS_6$ system. All of the micellar formulations were well tolerated and no significant changes were found in mouse body weights (Fig. 8B).

In addition to following changes in tumor sizes, the survivals of the treated mice were examined. As shown in Fig. 9, control mice with PBS treatment had a short survival time of around 18 days. Substantial survival advantage was observed in mice treated with PTX/POEG-*b*-PFTS mixed micelles. The median survival of mice in PTX/POEG-*b*-PFTS group (35 days) is significantly longer than that of Taxol (24 days, $P<0.05$) and blank micelles (25 days, $P < 0.05$). These results suggested that PTX/POEG-*b*-PFTS micelles could effectively inhibit the tumor growth and increase the survival of tumor-bearing mice.

4. Conclusions

In this work, we reported two well characterized POEG-*b*-PFTS prodrug micelle carriers ($POEG_{15}$-*b*-$PFTS_6$ and $POEG_{15}$-*b*-$PFTS_{16}$) that consist of multiple FTS-based hydrophobic domains and a POEG hydrophilic segment for efficient entrapment of water-insoluble chemotherapy drugs. Our POEG-*b*-PFTS prodrug micelles well retained the biological activity of FTS in vitro and showed significant tumor inhibition effect in a 4T1.2 mouse tumor model. Besides, these POEG-*b*-PFTS nanocarriers could efficiently penetrate into and accumulate at the tumors. Both carriers were effective in formulating PTX and demonstrated a slow kinetics of drug release. Finally, in vivo delivery of PTX via our prodrug carriers, particularly $POEG_{15}$-*b*-$PFTS_{16}$, led to significant inhibition of 4T1.2 tumors, much more effectively than carriers alone and Taxol. Future studies include more comprehensive evaluation of the therapeutic efficacy in various tumor models. The potential of POEG-*b*-PFTS nanocarriers in delivery of other anticancer agents will also be examined. Finally, the toxicity profiles of POEG-*b*-PFTS nanocarriers, particularly their biodegradability, will be studied.

Supplementary Material

Refer to Web version on PubMed Central for supplementary material.

Acknowledgments

This work was supported by NIH Grants No. RO1CA173887, No. R01GM102989, and No. R21CA173887.

References

1. Weiss RB, Donehower R, Wiernik P, Ohnuma T, Gralla R, Trump D, Baker J, Van Echo D, Von Hoff D, Leyland-Jones B. Hypersensitivity reactions from taxol. J Clin Oncol. 1990; 8:1263–1268. [PubMed: 1972736]
2. Feng SS, Chien S. Chemotherapeutic engineering: application and further development of chemical engineering principles for chemotherapy of cancer and other diseases. Chem Eng Sci. 2003; 58:4087–4114.

3. El-Rayes BF, Ibrahim D, Shields AF, LoRusso PM, Zalupski MM, Philip PA. Phase I study of liposomal doxorubicin (Doxil) and cyclophosphamide in solid tumors. Invest New Drugs. 2005; 23:57–62. [PubMed: 15528981]
4. Li C, Li S, Tu T, Qi X, Xiong Y, Du S, Shen Y, Tu J, Sun C. Paclitaxel-loaded cholesterol-conjugated polyoxyethylene sorbitol oleate polymeric micelles for glioblastoma therapy across the blood-brain barrier. Polym Chem. 2015; 6:2740–2751.
5. Vashist A, Vashist A, Gupta Y, Ahmad S. Recent advances in hydrogel based drug delivery systems for the human body. J Mater Chem B. 2014; 2:147–166.
6. Gu Y, Zhong Y, Meng F, Cheng R, Deng C, Zhong Z. Acetal-linked paclitaxel prodrug micellar nanoparticles as a versatile and potent platform for cancer therapy. Biomacromolecules. 2013; 14:2772–2780. [PubMed: 23777504]
7. Torchilin V. Tumor delivery of macromolecular drugs based on the EPR effect. Adv Drug Deliv Rev. 2011; 63:131–135. [PubMed: 20304019]
8. Duncan R, Vicent MJ. Polymer therapeutics-prospects for 21st century: the end of the beginning. Adv Drug Deliv Rev. 2013; 65:60–70. [PubMed: 22981753]
9. Lu J, Huang Y, Zhao W, Chen Y, Li J, Gao X, Venkataramanan R, Li S. Design and characterization of PEG-derivatized vitamin E as a nanomicellar formulation for delivery of paclitaxel. Mol Pharm. 2013; 10:2880–2890. [PubMed: 23768151]
10. Lu J, Huang Y, Zhao W, Marquez RT, Meng X, Li J, Gao X, Venkataramanan R, Wang Z, Li S. PEG-derivatized embelin as a nanomicellar carrier for delivery of paclitaxel to breast and prostate cancers. Biomaterials. 2013; 34:1591–1600. [PubMed: 23182923]
11. Chen Y, Zhang X, Lu J, Huang Y, Li J, Li S. Targeted delivery of curcumin to tumors via PEG-derivatized FTS-based micellar system. AAPS J. 2014; 16:600–608. [PubMed: 24706375]
12. Mi Y, Zhao J, Feng SS. Targeted co-delivery of docetaxel, cisplatin and herceptin by vitamin E TPGS-cisplatin prodrug nanoparticles for multimodality treatment of cancer. J Control Release. 2013; 169:185–192. [PubMed: 23403395]
13. Ma L, Kohli M, Smith A. Nanoparticles for combination drug therapy. ACS Nano. 2013; 7:9518–9525. [PubMed: 24274814]
14. Noh I, Kim HO, Choi J, Choi Y, Lee DK, Huh YM, Haam S. Co-delivery of paclitaxel and gemcitabine via CD44-targeting nanocarriers as a prodrug with synergistic antitumor activity against human biliary cancer. Biomaterials. 2015; 53:763–774. [PubMed: 25890771]
15. Rotblat B, Ehrlich M, Haklai R, Kloog Y. The Ras inhibitor farnesylthiosalicylic acid (Salirasib) disrupts the spatiotemporal localization of active Ras: a potential treatment for cancer. Methods Enzymol. 2008; 439:467–489. [PubMed: 18374183]
16. Niv H, Gutman O, Henis YI, Kloog Y. Membrane interactions of a constitutively active GFP-Ki-Ras 4B and their role in signaling evidence from lateral mobility studies. J Biol Chem. 1999; 274:1606–1613. [PubMed: 9880539]
17. Haklai R, Weisz MG, Elad G, Paz A, Marciano D, Egozi Y, Ben-Baruch G, Kloog Y. Dislodgment and accelerated degradation of Ras. Biochemistry. 1998; 37:1306–1314. [PubMed: 9477957]
18. Marom M, Haklai R, Ben-Baruch G, Marciano D, Egozi Y, Kloog Y. Selective inhibition of Ras-dependent cell growth by farnesylthiosalisylic acid. J Biol Chem. 1995; 270:22263–22270. [PubMed: 7673206]
19. Kloog Y, Cox AD. RAS inhibitors: potential for cancer therapeutics. Mol Med Today. 2000; 6:398–402. [PubMed: 11006529]
20. Gana-Weisz M, Halaschek-Wiener J, Jansen B, Elad G, Haklai R, Kloog Y. The Ras inhibitor S-trans, trans-farnesylthiosalicylic acid chemosensitizes human tumor cells without causing resistance. Clin Cancer Res. 2002; 8:555–565. [PubMed: 11839677]
21. Mor A, Aizman E, Kloog Y. Celecoxib enhances the anti-inflammatory effects of farnesylthiosalicylic acid on T Cells independent of prostaglandin E2 production. Inflammation. 2012; 35:1706–1714. [PubMed: 22688643]
22. Mor A, Aizman E, Chapman J, Kloog Y. Immunomodulatory properties of farnesoids: the new steroids? Curr Med Chem. 2013; 20:1218–1224. [PubMed: 23432580]

23. Riely GJ, Johnson ML, Medina C, Rizvi NA, Miller VA, Kris MG, Pietanza MC, Azzoli CG, Krug LM, Pao W. A phase II trial of Salirasib in patients with lung adenocarcinomas with KRAS mutations. J Thorac Oncol. 2011; 6:1435–1437. [PubMed: 21847063]
24. Badar T, Cortes JE, Ravandi F, O'Brien S, Verstovsek S, Garcia-Manero G, Kantarjian H, Borthakur G. Phase I study of S-trans, trans-farnesylthiosalicylic acid (salirasib), a novel oral RAS inhibitor in patients with refractory hematologic malignancies. Clinical Lymphoma Myeloma and Leukemia. 2015; 15:433–438.
25. Zhang X, Lu J, Huang Y, Zhao W, Chen Y, Li J, Gao X, Venkataramanan R, Sun M, Stolz DB, Zhang L, Li S. PEG-farnesylthiosalicylate conjugate as a nanomicellar carrier for delivery of paclitaxel. Bioconjug Chem. 2013; 24:464–472. [PubMed: 23425093]
26. Zhang X, Huang Y, Zhao W, Liu H, Marquez R, Lu J, Zhang P, Zhang Y, Li J, Gao X, Venkataramanan R, Xu L, Li S. Targeted delivery of anticancer agents via a dual function nanocarrier with an interfacial drug-interactive motif. Biomacromolecules. 2014; 15:4326–4335. [PubMed: 25325795]
27. Zhang X, Huang Y, Ghazwani M, Zhang P, Li J, Thorne SH, Li S. Tunable pH-responsive polymeric micelle for cancer treatment. ACS Macro Lett. 2015; 4:620–623.
28. Mi Y, Liu Y, Feng SS. Formulation of docetaxel by folic acid-conjugated d-α-tocopheryl polyethylene glycol succinate 2000 (Vitamin E TPGS 2k) micelles for targeted and synergistic chemotherapy. Biomaterials. 2011; 32:4058–4066. [PubMed: 21396707]
29. Aliabadi HM, Lavasanifar A. Polymeric micelles for drug delivery. Expert Opin Drug Deliv. 2006; 3:139–162. [PubMed: 16370946]
30. Huynh VT, de Souza P, Stenzel MH. Polymeric micelles with pendant dicarboxylato chelating ligands prepared via a michael addition for cis-platinum drug delivery. Macromolecules. 2011; 44:7888–7900.
31. Wang J, Sun J, Chen Q, Gao Y, Li L, Li H, Leng D, Wang Y, Sun Y, Jing Y. Star-shape copolymer of lysine-linked di-tocopherol polyethylene glycol 2000 succinate for doxorubicin delivery with reversal of multidrug resistance. Biomaterials. 2012; 33:6877–6888. [PubMed: 22770799]
32. Zhang X, Huang Y, Zhao W, Chen Y, Zhang P, Li J, Venkataramanan R, Li S. PEG-farnesyl thiosalicylic acid telodendrimer micelles as an improved formulation for targeted delivery of paclitaxel. Mol Pharm. 2014; 11:2807–2814. [PubMed: 24987803]
33. Du JZ, Du XJ, Mao CQ, Wang J. Tailor-made dual pH-sensitive polymer-doxorubicin nanoparticles for efficient anticancer drug delivery. J Am Chem Soc. 2011; 133:17560–17563. [PubMed: 21985458]
34. Li J, Yu F, Chen Y, Oupický D. Polymeric drugs: advances in the development of pharmacologically active polymers. J Control Release. 2015; 219:369–382. [PubMed: 26410809]
35. Delplace V, Couvreur P, Nicolas J. Recent trends in the design of anticancer polymer prodrug nanocarriers. Polym Chem. 2014; 5:1529–1544.
36. Smith D, Pentzer EB, Nguyen ST. Bioactive and therapeutic ROMP polymers. J Macromol Sci: Polym Rev. 2007; 47:419–459.
37. Hasegawa U, Van Der Vlies AJ, Wandrey C, Hubbell JA. Preparation of well-defined ibuprofen prodrug micelles by RAFT polymerization. Biomacromolecules. 2013; 14:3314–3320. [PubMed: 23937521]
38. Zuwala K, Smith AA, Postma A, Guerrero-Sanchez C, Ruiz-Sanchis P, Melchjorsen J, Tolstrup M, Zelikin AN. Polymers fight HIV: potent prodrugs identified through parallel automated synthesis. Adv Healthcare Mater. 2015; 4:46–50.
39. Smith AA, Wohl BM, Kryger MB, Hedemann N, Guerrero-Sanchez C, Postma A, Zelikin AN. Macromolecular prodrugs of ribavirin: concerted efforts of the carrier and the drug. Adv Healthcare Mater. 2014; 3:1404–1407.
40. Mynar JL, Goodwin AP, Cohen JA, Ma Y, Fleming GR, Frechet JMJ. Two-photon degradable supramolecular assemblies of linear-dendritic copolymers. Chem Commun. 2007:2081–2082.
41. Klaikherd A, Nagamani C, Thayumanavan S. Multi-stimuli sensitive amphiphilic block copolymer assemblies. J Am Chem Soc. 2009; 131:4830–4838. [PubMed: 19290632]

42. Huang Y, Lu J, Gao X, Li J, Zhao W, Sun M, Stolz DB, Venkataramanan R, Rohan LC, Li S. PEG-derivatized embelin as a dual functional carrier for the delivery of paclitaxel. Bioconjug Chem. 2012; 23:1443–1451. [PubMed: 22681537]

43. Zhang P, Huang Y, Liu H, Marquez RT, Lu J, Zhao W, Zhang X, Gao X, Li J, Venkataramanan R, Li S. A PEG-Fmoc conjugate as a nanocarrier for paclitaxel. Biomaterials. 2014; 35:7146–7156. [PubMed: 24856103]

44. Cho H, Indig GL, Weichert J, Shin HC, Kwon GS. In vivo cancer imaging by poly (ethylene glycol)-b-poly (ε-caprolactone) micelles containing a near-infrared probe. Nanomedicine: NBM. 2012; 8:228–236.

Statement of significance

Polymerization of drug-based monomer represents a facile and precise method to obtain well-defined polymeric prodrug amphiphiles. Currently, most reports largely focus on the synthesis methods and the biophysical properties. There is limited information about their anti-tumor activity and delivery function as prodrug carriers *in vitro* and *in vivo*. In this manuscript, we report the development of two novel prodrug copolymers, $POEG_{15}$-*b*-$PFTS_6$ and $POEG_{15}$-*b*-$PFTS_{16}$ composed of hydrophilic poly(oligo(ethylene glycol) methacrylate) (POEG) and hydrophobic farnesylthiosalicylate (FTS, a nontoxic Ras antagonist) blocks. Both POEG-*b*-PFTS polymers were able to self-assemble into nano-sized micelles with intrinsic antitumor activity *in vitro* and *in vivo*. More importantly, POEG-*b*-PFTS polymers were effective in forming stable mixed micelles with various anticancer agents including PTX, DOX, docetaxel, gefitinib, and imatinib. Delivery of PTX via our new carrier led to significantly improved antitumor activity, suggesting effective PTX/FTS combination therapy. We believe that our study shall be of broad interest to the readers in the fields of biomaterials and drug delivery.

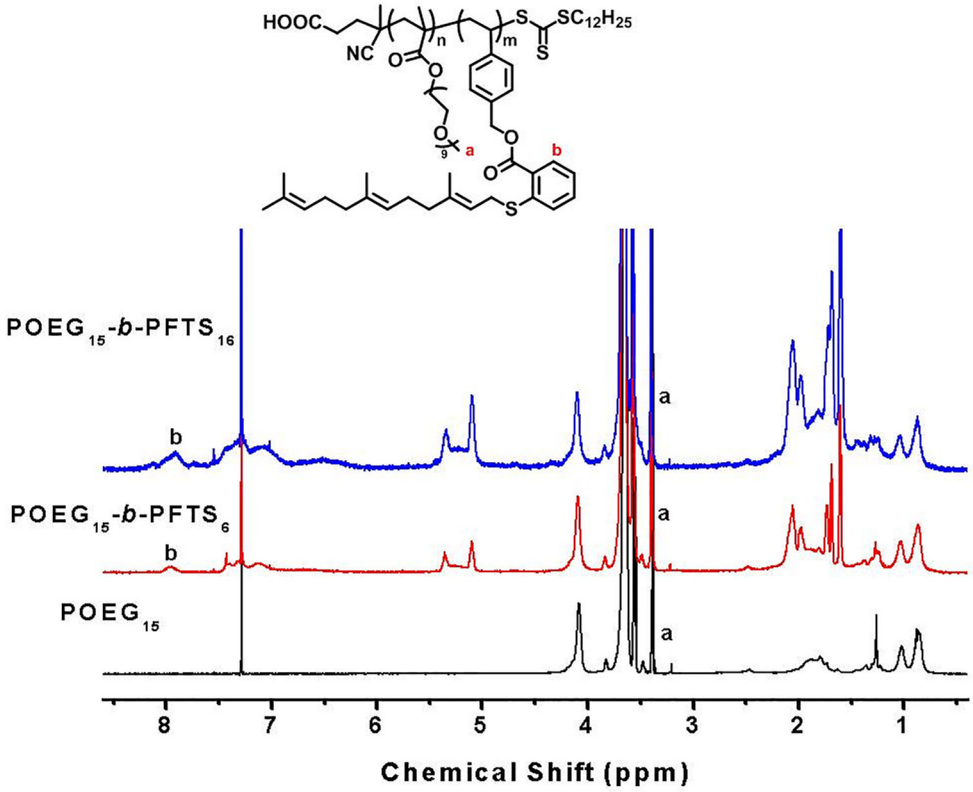

Fig. 1.

^{1}H NMR spectra of the $POEG_{15}$, $POEG_{15}$-*b*-$PFTS_6$ and $POEG_{15}$-*b*-$PFTS_{16}$ polymers in $CDCl_3$.

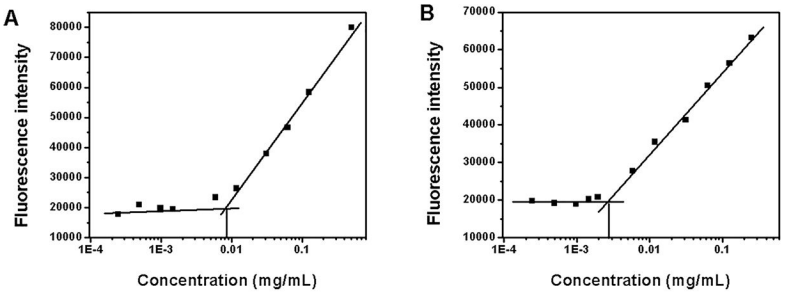

Fig. 2.

Plots of fluorescence intensity at 650 nm versus concentrations of $POEG_{15}$-*b*-$PFTS_6$ (A) and $POEG_{15}$-*b*-$PFTS_{16}$ copolymers.

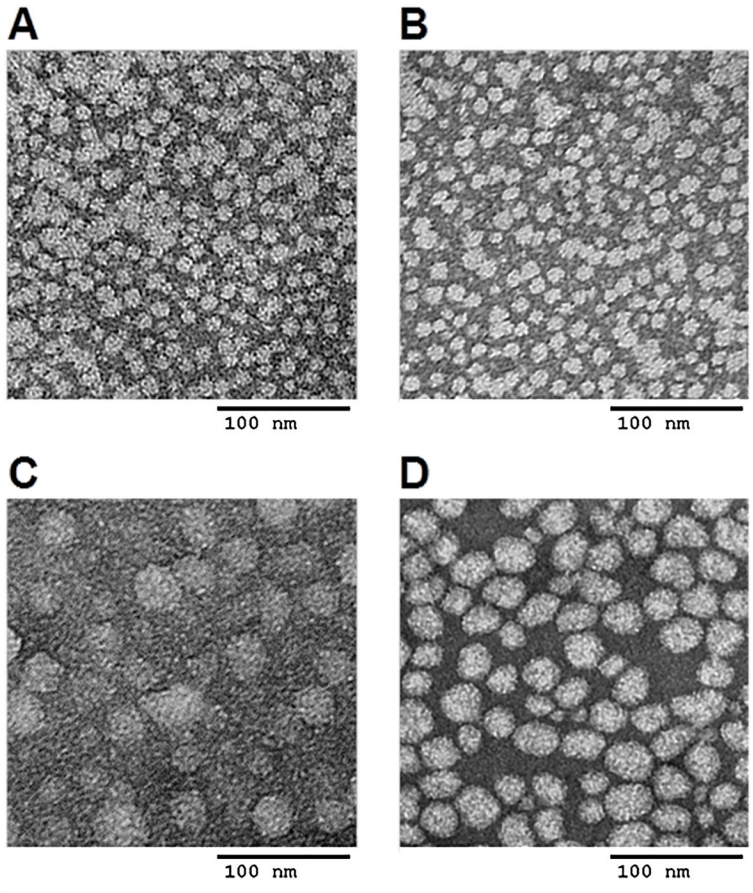

Fig. 3.

TEM images of PTX-free $POEG_{15}$-*b*-$PFTS_6$ micelles (A) and $POEG_{15}$-*b*-$PFTS_{16}$ micelles (C), and PTX-loaded $POEG_{15}$-*b*-$PFTS_6$ micelles (B) and $POEG_{15}$-*b*-$PFTS_{16}$ micelles (D) using negative staining. Scale bar is 100 nm.

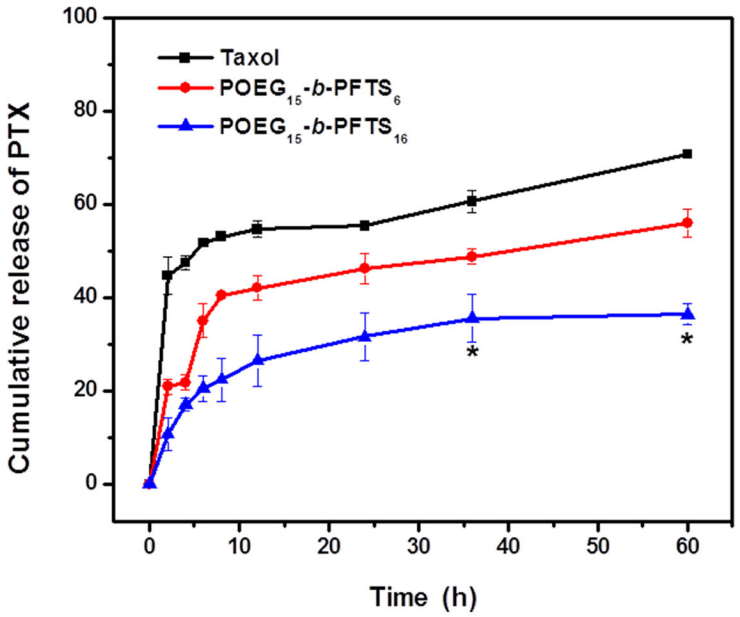

Fig. 4.

Cumulative PTX release profile from two PTX-loaded POEG-*b*-PFTS micelles with Taxol as the control. PBS containing 0.5% (w/v) Tween 80 was used as the release medium. PTX concentration was fixed at 1 mg PTX/mL. Values reported are the means ± SD for triplicate samples. *P < 0.05 ($POEG_{15}$-*b*-$PFTS_{16}$ vs Taxol).

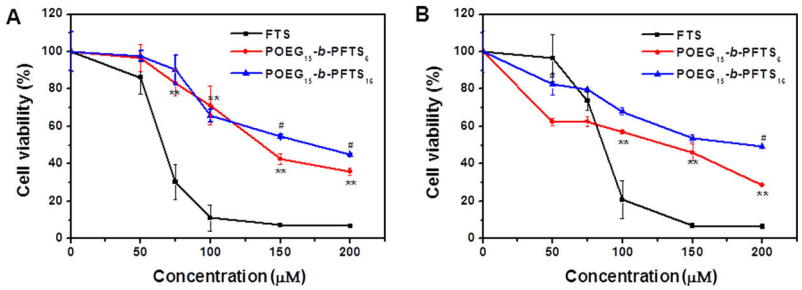

Fig. 5.

MTT cytotoxicity of two POEG-*b*-PFTS prodrug micelles in 4T1.2 mouse breast cancer cell line (A) and DU-145 human prostate cancer cell line (B) with free FTS as the control. Cells were treated with different micelles for 72 h and values reported are the means ± SD for triplicate samples. $^{*}P < 0.05$, $^{**}P < 0.01$ ($POEG_{15}$-*b*-$PFTS_6$ vs FTS); $^{\#}P < 0.05$, $^{\#\#}P < 0.01$ ($POEG_{15}$-*b*-$PFTS_6$ vs $POEG_{15}$-*b*-$PFTS_{16}$).

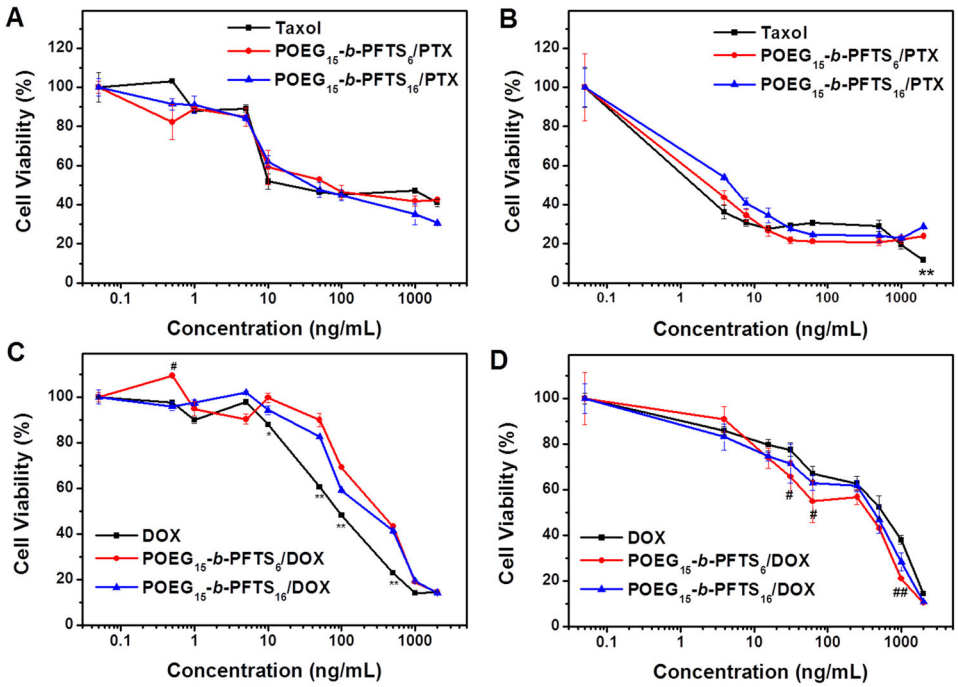

Fig. 6.

MTT cytotoxicity assay of PTX-loaded POEG-*b*-PFTS micelles in 4T1.2 (A) and DU-145 cell line (B), and DOX-loaded POEG-*b*-PFTS micelles in 4T1.2 (C) and DU-145 cell line (D) after 72 h treatment. Data are presented as the means ± SD for triplicate samples. $^{*}P < 0.05$, $^{**}P < 0.01$ (POEG-*b*-PFTS/PTX vs Taxol, POEG-*b*-PFTS/DOX vs DOX); $^{\#}P < 0.05$, $^{\#\#}P < 0.01$ ($POEG_{15}$-*b*-$PFTS_6$/DOX vs DOX).

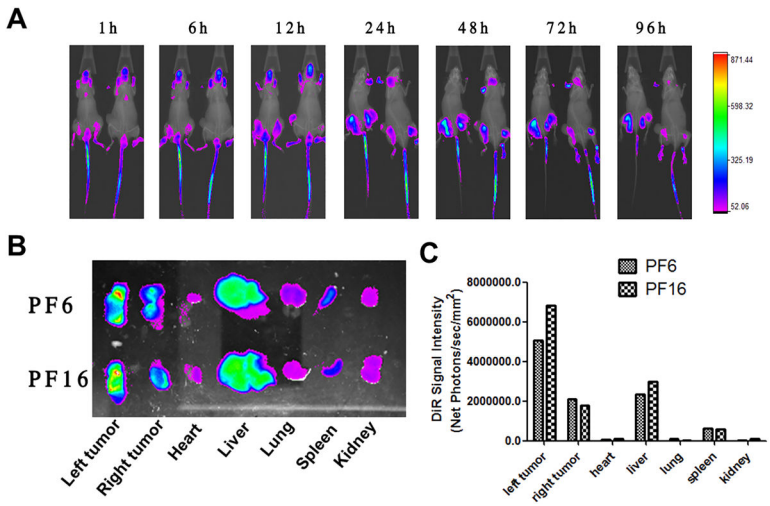

Fig. 7.

(A) *In vivo* and (B) *ex vivo* NIRF imaging of DiR-loaded $POEG_{15}$-*b*-$PFTS_6$ and $POEG_{15}$-*b*-$PFTS_{16}$ micelles (denoted as PF6 and PF16) in prostate cancer PC-3 xenograft-bearing mice. (C) Quantitative fluorescence intensities of tumors and major organs from *ex vivo* images.

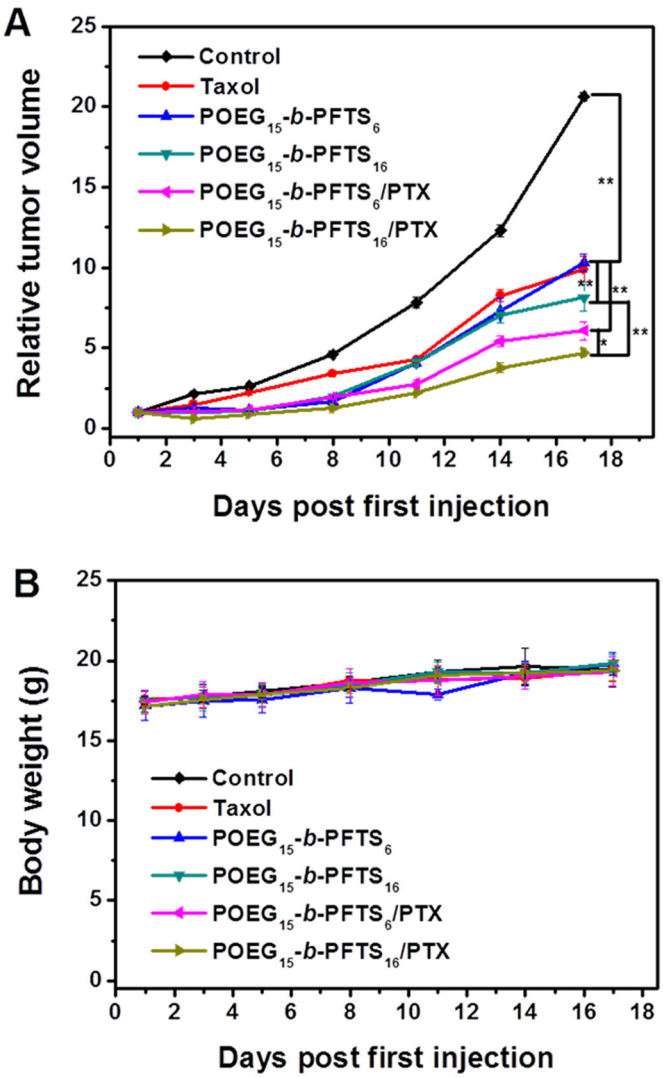

Fig. 8.

(A) Antitumor activity of Taxol, POEG-*b*-PFTS prodrug micelles and PTX-loaded POEG-*b*-PFTS micelles in a syngeneic murine breast cancer model (4T1.2). Five injections were given on days 1, 2, 5, 8 and 11 and each point represents the mean of tumor size (n = 5). *P < 0.05; **P < 0.01. (B) Changes of body weight in mice receiving different treatments.

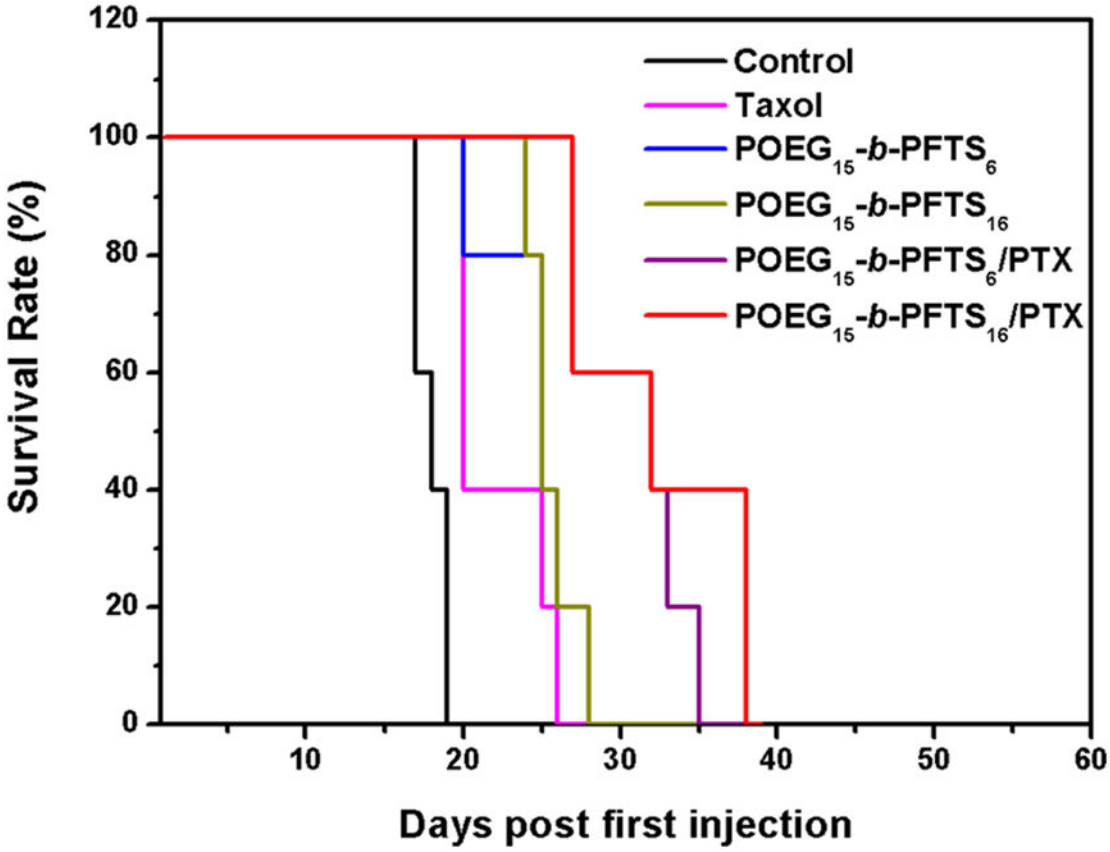

Fig. 9.

Kaplan-Meier survival curves for 4T1.2 tumor-bearing mice receiving different treatments. Mice were treated with Taxol, POEG-*b*-PFTS prodrug micelles, PTX-loaded POEG-*b*-PFTS micelles, and saline on days 1, 3, 5, 8, 11 respectively.

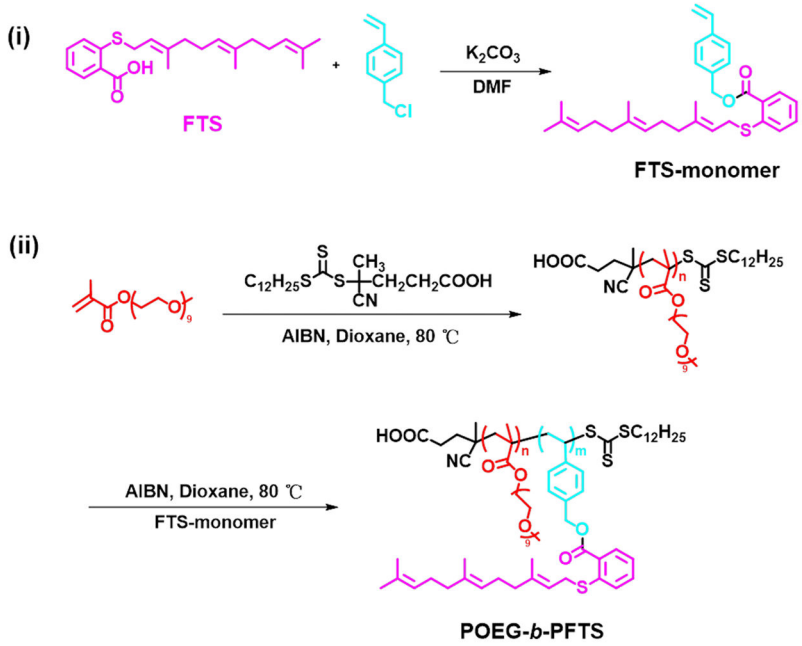

Scheme 1.
Synthesis of the FTS-monomer and POEG-*b*-PFTS polymers via RAFT polymerization.

Table 1

Characterizations of the $POEG_{15}$ Macro-RAFT agent, $POEG_{15}$-*b*-$PFTS_6$ and $POEG_{15}$-*b*-$PFTS_{16}$ block copolymers.

Block compolymer	Monomer conversion[a]	Hydrophilic/Hydroph obic ratio[b]	M_n[a] (NMR)	M_n[c] (GPC)	M_w[c] (GPC)	M_w/M_n[c] (GPC)
$POEG_{15}$	75	-	7500	7130	8140	1.14
$POEG_{15}$-*b*-$PFTS_6$	75	7500/2844	10700	9160	10260	1.12
$POEG_{15}$-*b*-$PFTS_{16}$	70	7500/7584	15500	13700	17600	1.30

Notes:

[a] Calculated by NMR results.

[b] The block molecular weight ratio of OEG/FTS in polymers.

[c] Measured by GPC with THF as the eluent, and the molecular weights and their distribution were calculated with polystyrene standards.

Table 2

Size, CMC and FTS loading capacity of $POEG_{15}$-*b*-$PFTS_6$ and $POEG_{15}$-*b*-$PFTS_{16}$ micelles

Micelles	Size (nm)[a]	PDI[b]	DLC(%)[c]	CMC[d] (mg/L)
$POEG_{15}$-*b*-$PFTS_6$	39.2 ± 0.4	0.26 ± 0.01	20.1	8.6
$POEG_{15}$-*b*-$PFTS_{16}$	138.7 ± 3.3	0.33 ± 0.04	36.7	2.7

[a] Measured by dynamic light scattering particle sizer.

[b] PDI = polydispersity index.

[c] FTS loading capacity.

[d] CMC = critical micelle concentration.

Table 3

Physicochemical characterizations of PTX-loaded PEG-*b*-FTS micelles.

Micelles	Mass ratio (mg: mg)[a]	Size (nm)[b]	PDI[c]	DLC(%)[d]	DLE(%)[e]	Stability[f]
$POEG_{15}$-*b*-$PFTS_6$: PTX	10: 1	32.8 ± 0.3	0.26 ± 0.01	4.6	51.1	5 d
$POEG_{15}$-*b*-$PFTS_6$: PTX	15: 1	32.8 ± 0.2	0.24 ± 0.02	4.3	68.7	8 d
$POEG_{15}$-*b*-$PFTS_6$: PTX	30: 1	37.8 ± 0.2	0.34 ± 0.03	2.8	87.4	12 d
$POEG_{15}$-*b*-$PFTS_{16}$: PTX	10: 1	115.6 ± 1.9	0.32 ± 0.04	8.2	90.5	9 d
$POEG_{15}$-*b*-$PFTS_{16}$: PTX	15: 1	113.9 ± 2.1	0.32 ± 0.04	5.4	85.9	13 d
$POEG_{15}$-*b*-$PFTS_{16}$: PTX	30: 1	130.6 ± 1.7	0.39 ± 0.03	3.1	96.7	23 d

[a] PTX concentration in micelles was kept at 1 mg/mL.

[b] Measured by dynamic light scattering particle sizer.

[c] PDI = polydispersity index.

[d] DLC = drug loading capacity.

[e] DLE = drug loading efficiency.

[f] Data mean that there was no noticeable PTX precipitation during the follow-up period at 4 °C.